THE JOURNAL OF COMPARATIVE NEUROLOGY 486:361–372 (2005)

Topography of Pig Retinal Ganglion Cells

MÓNICA GARCÍA, JAVIER RUIZ-EDERRA, HENESTO HERNÁNDEZ-BARBÁCHANO, AND ELENA VECINO*
Department of Cell Biology, Faculty of Medicine, University of the Basque Country, E-48940 Leioa, Vizcaya, Spain

ABSTRACT

In the present work we analyzed the distribution of retinal ganglion cells (RGCs) in the pig retina. RGCs were retrogradely labeled in vivo by injecting Fluoro-Gold into the optic nerve. RGC density and the distribution of RGCs in terms of soma size were analyzed. Different regions of the porcine retina were identified following analysis of the distribution of RGCs in terms of cell density and soma size: in the central retina, we found a high-density horizontal RGC band lying dorsal to the optic disc. Moreover, in this region, a high proportion of RCGs with small soma size was observed. From the central to the more peripheral retina, we observed a decrease in RGC density, together with a greater presence of RGCs with larger somas. The results of this study should prove to be useful as a foundation for future studies with the porcine retina as a model in ophthalmic research. The study also highlights the necessity to label the RGC population specifically with retrograde tracers in order to quantify precisely alterations in the cell population associated with experimental treatments. J. Comp. Neurol. 486:361–372, 2005.

Indexing terms: porcine; neuronal tracing; Fluoro-Gold; RGC; cell size; cell density; retina

Retinal ganglion cells (RGCs) are the output neurons of the retina, decoding and conveying visual information along the optic nerve to the brain. These cells are specifically affected in pathologies such as glaucoma, retinal ischemia, and diabetic retinopathy (Glovinsky et al., 1991; Vickers et al., 1995; Wygnanski et al., 1995; Selles-Navarro et al., 1996; Zhang et al., 1998; Joo et al., 1999; Lieth et al., 2000). However, the mechanisms that lead to selective RGC death associated with these pathologies remain unknown.

To study the etiology of such pathologies affecting human vision, it is essential to use an adequate model, which is relevant to the human visual system. Although nonhuman primates are considered the best substitutes for humans in visual science experimentation, both the expense and the availability of these species limit their use. In the present work, we have focused on the pig as an appropriate model, on the basis of the following interesting features: 1) the anatomy of the eye and the structure of the pig retina are very similar to those of humans (Prince et al., 1960; Beauchemin, 1974; De Schaepdrijver et al., 1990; McMenamin and Steptoe, 1991; Olsen et al., 2002; Ruiz-Ederra et al., 2003, 2004); 2) the immune system is well characterized; 3) tools employed for diagnostics in ophthalmology, such as optical coherence tomography, corneal topography imaging, or multifocal electroretinogram, can be applied to pig eye, supporting the use of this animal as a good model for ophthalmological studies (Kyhn et al., 2004; Maverick et al., 2004; van Velthoven et al., 2004); and 4) it is possible to reproduce ocular diseases in pigs similar to those found in humans (Li et al., 1998), and the porcine retina seems to be a good model for study of the pathophysiology of diseases affecting RGCs (Komáromy et al., 2003). Despite its obvious interest, there are few studies describing the distribution of RGCs in the

Mónica García and Javier Ruiz-Ederra contributed equally to this work.

Grant sponsor: The American Glaucoma Foundation; Grant sponsor: European Community; Grant number: QLK6-CT-2001-00385; Grant sponsor: European Community postdoctoral fellowship (to M.G.); Grant sponsor: Spanish Ministry of Science and Technology; Grant number: BFI 2003-07177; Grant sponsor: University of the Basque Country; Grant number: E-14887/2002; Grant number: E-15350/2003; Grant sponsor: Jesús de Gangoiti Barrera Foundation (to J.R.-E.). Grant sponsor: ONCE's award 2004.

*Correspondence to: Elena Vecino, Department of Cell Biology, Faculty of Medicine, University of the Basque Country, E-48940 Leioa, Vizcaya, Spain.

E-mail: gcpvecoe@lg.ehu.es

Received 20 May 2004; Revised 13 July 2004; Accepted 20 January 2005

DOI 10.1002/cne.20516

Published online in Wiley InterScience (www.interscience.wiley.com).

porcine retina and comparing this distribution with that found in the human retina.

Despite it not being feasible to classify RGCs exclusively in terms of soma size, evidence indicates that, in the cat retina, RGC soma size is closely related to cellular properties, such as receptive field organization, number and distribution of dendrites, morphology, and central projections (Boycott and Wässle, 1974; Stone and Clarke, 1980; Rowe and Dreher, 1982). The presence of subgroups of RGCs based on soma size has been reported for a variety of mammalian retinas, such as the cat (Stone, 1965, 1978; Boycott and Wässle, 1974; Wässle and Illing, 1980; Chen and Weber, 2001) and the primate retina, including that of humans (Stone and Johnston, 1981; Yamada et al., 1996). However, the presence of these size-based subgroups in the rat retina remains controversial (Fukuda, 1977; Luo et al., 2001).

Even though some studies point toward a nonselective loss of cells in terms of RGC size (Kalloniatis et al., 1993; Graham et al., 1996; Morgan et al., 2000), it has been widely documented that RGCs are differentially affected during ocular pathologies, in a size-dependent manner. Thus, large RGCs have been found to be more susceptible to death in human glaucoma (Quigley et al., 1987, 1988, 1989) and in monkey experimental glaucoma (Glovinsky et al., 1991). Moreover, previous in vitro studies performed in our laboratory have demonstrated that, in the pig retina, a differential survival capacity was associated with three different RGC sizes (García et al., 2002). In addition, large porcine RGCs in vitro have been reported to be more susceptible to excitotoxic insults induced by glutamate (Luo et al., 2001).

The object of the present work was to characterize in detail the density and soma size distribution of Fluoro-Gold-prelabeled porcine RGCs. In addition, we compared the number of RGCs stained with the classical Nissl staining method vs. the specific RGC retrograde labeled Fluoro-Gold method. Knowledge of the precise topographic distribution of adult porcine RGCs will facilitate the development of new models of retinal injuries affecting RGCs, involving a large mammal that closely resembles the human being.

MATERIALS AND METHODS

Tissue collection

Retinas from the left eyes of seven adult pigs (*Sus scrofa*) were used in the present work. All experimental methods and animal care procedures adhered to the ARVO Statement for the Use of Animals in Ophthalmic and Vision Research and were approved by the local Institutional Animal Care and Use Committee (IACUC). Pigs were deeply anesthetized with an intramuscular injection of ketamine hydrochloride (Ketolar) + Diazepan (20 mg/kg each). Once the animal was anesthetized, an intravenous cannula was applied to the ear to provide the animal with Propofol (1 ml every 15 minutes), an additional anesthetic, which maintained deep anesthesia throughout the operation. A life-support machine was used to facilitate breathing and to monitor vital functions during the operation.

RGC back-filling

RGCs from five left eyes were back-filled with 3% Fluoro-Gold (Fluorochrome, Englewood, CO) diluted in a solution containing 0.9% NaCl and 0.1% dimethylsulfoxide. Forty microliters of Fluoro-Gold was injected into the optic nerve about 4 mm from the optic nerve head. Pigs were kept alive for 2 days postoperation to allow Fluoro-Gold to fill the entire population of RGCs. Then animals were euthanized with an overdose of anesthesia, the eyes were enucleated, and the lens and vitreous were extracted by cutting the anterior chamber at the level of the ora serrata. The eyecups were fixed with 4% paraformaldehyde in 0.1 M phosphate-buffered saline (PBS; pH 7.4) for 4 hours at 4°C, and then retinas were removed and flat-mounted with the RGC layer being uppermost. They were then coverslipped with phosphate-buffered saline (PBS)/glycerin (1:1), so that shrinkage did not occur during the processing of the tissue.

Nissl staining

Two porcine retinas were stained with 1% toluidine blue following the Nissl method as described by Hebel (1976) for the pig retina.

Image capture

Images from each retina were obtained by using an epifluorescence microscope (Axioskop 2; Zeiss, Jena, Germany) coupled to a digital camera (CoolSnap; RS Photometrics, Tucson, AZ). The images were captured in a systematic way, by using the optic disc (OD) as a reference point. Two imaginary perpendicular lines, through the X and Y axis, both of them crossing the OD, were drawn, thus dividing the pig retina into different subregions: dorsal (D), ventral (V), temporal (T), and nasal (N), and quadrants resulting from the combination of these (nasal-dorsal, ND; temporal-dorsal, TD; nasal-ventral, NV; and temporal-ventral, TV). We recorded one of four ×40 microscopic fields following the imaginary X and Y lines as references. We recorded 100–130 fields/retina, and the distance between each sampling point was 2.3 mm. We captured each retinal field at different sampling points, shown as open circles in Figure 1, resulting from running the entire retina through the X axis (letters) and Y axis (numbers; from 1A at the OD to 8H at the periphery). The sampling area recorded represented 1.4% of the mean area of the five retinas analyzed. This sample size has previously been reported to represent a significant percentage of the retina (Peinado-Ramón et al., 1996). Moreover, we captured additional samples from retinal areas with an especially high density of RGCs in order to have a statistically significant sample from this region. Drawings of pig retinas representing isodensity profiles and the distribution of RGCs were made in Adobe Photoshop 5.0. Measurement of the total retinal area, retinal regions, and other parameters were performed with the aid of Spot Advanced software (Diagnostic Instruments Inc., Sterling Heights, MI), in order to 1) estimate the number of RGCs present in different retinal regions or the total number of RGCs (by multiplying the area of a particular retinal region by its corresponding RGC mean density) and 2) to measure retinal distances such as the distance different retinal regions and the OD.

Morphometric analysis

For each recorded retinal field, we quantified the number of RGCs and measured the soma major axis length and soma area of each of the RGCs present. Analysis of these parameters was performed with a digital palette

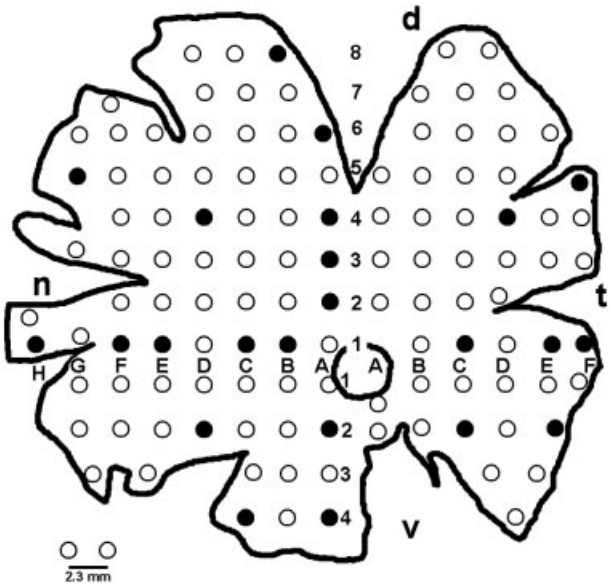

Fig. 1. Schematic representation of a whole-mounted pig retina, showing the localization of the different retinal fields analyzed. Two imaginary perpendicular axis, the X axis (represented by letters) and the Y axis (represented by numbers), both of them intersecting at the optic disc, were used as references in order to perform the systematic capture of 100–130 fields by running the entire retina through both axes. The distance between one sampling point and the next was 2.3 mm. Sample points are represented by open circles, whereas solid circles represent the retinal points from which histograms shown in Figure 4 were obtained. d, dorsal; n, nasal; t, temporal; v, ventral. Scale bar = 2.3 mm.

(Easypen, Genius) in combination with image-analysis software (Scion Image; Scion, Frederick, MD). Each RGC soma was filled out directly on the computer screen, and data thus obtained were transferred to a data sheet for subsequent statistical analysis.

RGC density was calculated by taking into consideration the size of the field captured by the digital camera at $\times 40$ (0.08 mm^2) and the number of RGCs present in the field. The mean RGC soma area in each field analyzed was also calculated. Furthermore, we studied the RGC soma size distribution as a function of eccentricity from the OD. To this end, we selected 25 fields/retina located at different eccentricities from the OD, represented as solid circles in Figure 1. For each field of the five retinas, we counted the number of RGCs with a given major axis length value, and frequencies were represented by histograms.

Finally, on the basis of size distribution, we classified the RGCs into three categories to test whether different-sized RGCs were distinctly distributed within the retina, by analyzing the percentage of these groups of cells in all retinal fields. We considered the presence of three groups of RGCs, attending to the length of their soma major axis. Thus we considered them as being small (<15 μm), medium-sized (15–20 μm), or large (>20 μm). The percentage of each RGC size group was calculated in each of the fields captured.

The proposed classification of RGCs is based exclusively on soma size and is not a functional classification. It is important to remember that RGCs with different soma sizes can be carrying out different physiological tasks and that RGCs with similar soma sizes can have different functional roles. Nevertheless, we employed this classification scheme to facilitate the handling of the huge volume of data analyzed in the present work (45,800 RGCs).

Data concerning RGC parameters were collected from five retinas, and corresponding mean values were obtained with SPSS software (SPSS, Chicago, IL). Subsequently, we plotted out the mean density and RGC soma size distribution on color-coded or size-distribution maps representing the pig retina. RGC density, mean soma area, and percentage of size groups were expressed as mean ± SEM. Mean data from different retinas, regions, and subregions were compared with one-way ANOVA followed by the Scheffé test to compare two groups. Comparison of results obtained from Nissl staining and Fluoro-Gold methods was performed by using the Student's *t*-test. The minimal level of significant difference was defined as $P < 0.05$.

RESULTS

Gross anatomy of the pig retina

The mean area of the porcine retina (781 ± 40 mm^2) is similar to that of the human retina (Stone and Johnston, 1981). However, the pig OD is not located in the center of the retina (Fig. 2), so the mean area of the dorsal retina (462 ± 27 mm^2) was found to be about threefold larger than that of the ventral retina (172 ± 23 mm^2), whereas the mean area of the nasal retina was 1.6-fold larger (480 ± 32 mm^2) than that of the temporal retina (301 ± 30 mm^2).

Distribution of RGCs (Fluoro-Gold method)

In the present study, we counted and measured a total of 45,800 RGCs from five pig retinas. The mean number of RGCs per retina was estimated to be 583,871 ± 42,658. However, RGCs were not distributed homogeneously throughout the retina. Thus, by attending to RGC density, mean soma area, and soma size distribution, we distinguished three regions in the retina: the visual streak, the midperiphery, and the periphery.

The visual streak consisted of a high-density RGC horizontal band, which constantly lies dorsal to the OD, running from the nasal to the temporal extreme above the OD. This retinal landmark of 2.5 mm width was easily discernible at low magnification. In the visual streak, we found the highest RGC density, the lowest mean soma area, and a normal distribution of RGCs, by attending to soma sizes. This band, which represented only 7% of the total area of the retina, contained 24.5% of all RGCs (143,243 ± 13,243; Table 1, Fig. 3).

We considered the midperiphery as being a vast region located between the visual streak and the periphery. Here we found medium RGC density and medium soma mean area, whereas soma sizes were distributed in a plurimodal fashion. This region represented 78% of the total retinal area and contained 70.5% of RGCs (411,439 ± 36,715; Table 1, Fig. 3).

Finally, we defined the periphery as a ring in the outer edge of the retina measuring ~1.5 mm width in the dorsal retina and ~3.5 mm width in the ventral retina. This was found to be the region with the lowest RGC density and the highest mean soma area and showed a plurimodal distribution of soma sizes. Thus, this region, making up

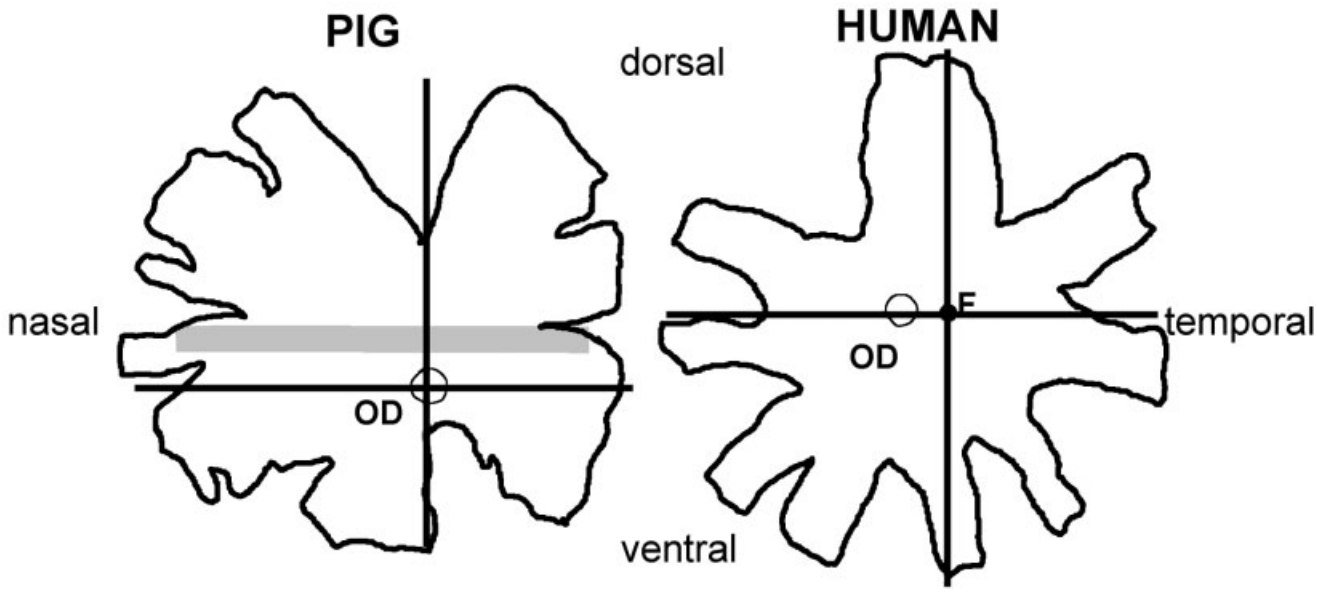

Fig. 2. Schematic representations of pig and human whole-mounted retinas. The reference landmarks used to analyze porcine retina (left) and to study the human retina (right; Stone and Johnston, 1981; Curcio and Allen, 1990) are shown. Drawings are not at the same scale. The drawing of the human retina is a modification of that by Stone and Johnston (1981). OD, optic disc; F, fovea.

TABLE 1. Summary of Results of Morphometric Analysis and Sampling Estimations for the Porcine Retina[1]

	Mean RGC density (RGCs/mm^2)				Retinal area (mm^2)				Estimated RGC number[3]				Sample size[4]	
Eye[2]	VS	MP	P	Total mean density	VS	MP	P	Total	VS	MP	P	Total	No. fields	Percentage at retina
3	1,828 ± 222	560 ± 34	313 ± 39	839 ± 82	60	589	113	762	109,680	329,840	35,369	474,889	110	1.4
12	2,719 ± 252	717 ± 47	175 ± 28	1,199 ± 117	57	765	118	940	154,983	548,505	20,650	724,138	130	1.3
29	2,584 ± 321	704 ± 42	162 ± 46	1,153 ± 126	46	553	125	724	118,864	389,312	20,250	528,426	100	1.3
43	3,275 ± 415	722 ± 45	237 ± 31	1,278 ± 154	56	568	125	749	183,400	410,096	29,625	623,121	115	1.4
44	2,871 ± 436	680 ± 51	331 ± 72	1,208 ± 153	52	558	121	731	149,292	379,440	40,051	568,783	116	1.5
Mean	2,641 ± 149	678 ± 20	241 ± 19	1,133 ± 57	54	607	120	781	143,243	411,439	29,189	583,871	114	1.4

[1]VS, visual streak; MP, midperiphery; P, periphery; RGCs, retinal ganglion cells.
[2]Numbers of the eyes analyzed in the present work.
[3]Using the values present in columns 2 and 3, we estimated the RGC number in each retinal subregion as well as in the whole retina.
[4]Number of fields analyzed and the percentages of the total retinal surface that they represent.

15% of the retinal area, contained only 5% of RGCs (29,189 ± 3,931; Table 1, Fig. 3).

RGC density

Variability in the density of RGCs among the five porcine retinas was found to be low. Thus, the mean value of RGC density was 1,133 ± 57 RGCs/mm^2, with no significant differences among retinas ($P = 0.113$). However, statistical analysis showed that RGC density was significantly different ($P < 0.01$) among different regions of the pig retina. The region with highest RGC density was the visual streak (2,641 ± 149 RGCs/mm^2), followed by the midperiphery (678 ± 20 RGCs/mm^2) and finally the periphery, with the lowest density of RGCs (241 ± 19 RGCs/mm^2; Table 2).

Within the visual streak, different subregions can be identified on the basis of RGC density. At its central region (about 1.2 mm from the optic disc), we found a *subband* with a high mean RGC density of 4,331 ± 231 RGCs/mm^2. About 8.5 mm temporally to the OD, we found a small circular area (with a diameter of ~250 μm), where RGCs density peaked to 5,735 ± 1,066 RGCs/mm^2. Additionally, we found an additional peak in RGC density in the nasal arm of the visual streak, located about 6.5 mm nasally to the OD, with a similar mean density of 5,658 ± 290 RGCs/mm^2 (Fig. 3A). We will refer to these areas as the area centralis.

The distribution of RGCs along the midperiphery was not homogeneous. Thus, when we compared RGC density in the different subregions of the midperiphery retina, we found significant differences between them. Similarly, RGC density in the periphery was heterogeneous (Table 2, Fig. 3A).

RGC mean soma area

The mean soma area (in square micrometers) of RGCs was larger in regions of lower RGC density and smaller in regions of higher RGC density. This cellular parameter was significantly different ($P < 0.01$) among the three retinal regions. Thus, we found the smallest values of mean RGC area in the visual streak (214 ± 5 μm^2), fol-

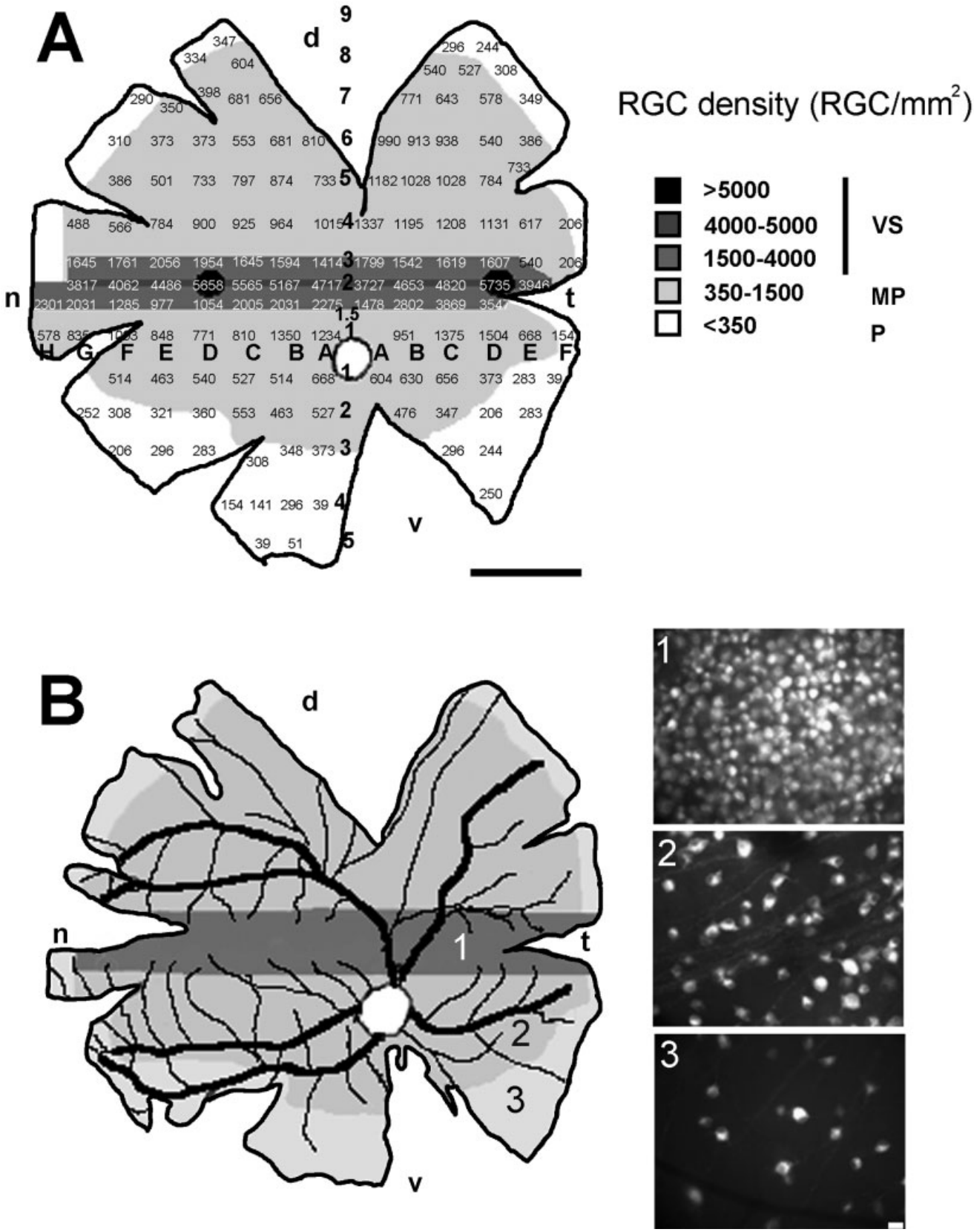

Fig. 3. Representations of pig retina whole mounts, showing retinal ganglion cell (RGC) densities in the different analyzed fields. **A:** Mean values of RGC density (in RGCs/mm^2) in the different fields of the five retinas analyzed. The five gray values represent RGC isodensity groups (see key). VS, visual streak; MP, midperiphery; P, periphery. **B:** Map of the pig retina showing the three main retinal regions: the visual streak (black), the midperiphery (gray), and the periphery (pale gray). The images to the right illustrate Fluoro-Gold-prelabeled RGCs in the visual streak (1), the midperiphery (2), and the periphery (3) of the retina. A representation of the typical retinal vascular pattern is also shown. d, dorsal; n, nasal; t, temporal; v, ventral. Scale bars = 5 mm in A (applies to A,B); 20 μm in B1–3.

TABLE 2. Porcine Retinal Ganglion Cell Mean Density[1] (RGCs/mm^2)

Region	Subregion		Quadrants		Total
Visual streak					2,641 ± 149
Midperiphery	Dorsal	823 ± 24	ND	763 ± 29	678 ± 20**
	Ventral	422 ± 18‡‡	TD	887 ± 39 ‖	
	Nasal	616 ± 22	NV	422 ± 19 ‖ ‖ # #	
	Temporal	762 ± 35§§	TV	422 ± 38 ‖ ‖ # #	
Periphery	Dorsal	292 ± 25	ND	344 ± 42	241 ± 19**††
	Ventral	166 ± 23‡‡	TD	250 ± 28	
	Nasal	262 ± 30	NV	181 ± 32 ‖	
	Temporal	218 ± 23	TV	140 ± 28 ‖ ‖	

[1]Mean RGC density in the different subregions and quadrants of regions of the porcine retina. To the right, mean RGC density in the whole region is shown. Values are expressed as mean ± SEM of the number of RGCs mm^2. ND, nasodorsal; TD, temporal-dorsal; NV, nasoventral; TV, temporal-ventral.
**$P < 0.01$ with respect to the visual streak.
††$P < 0.01$ with respect to the midperiphery.
‡‡$P < 0.01$ with respect to dorsal.
§§$P < 0.01$ with respect to nasal.
‖$P < 0.05$ and ‖ ‖$P < 0.01$ with respect to ND.
#$P < 0.01$ with respect to TD.

TABLE 3. Mean Porcine RGC Soma Area[1] (μm^2)

Region	Subregion		Quadrants		Total
Visual streak					214 ± 5
Midperiphery	Dorsal	266 ± 3	ND	258 ± 3	274 ± 3**
	Ventral	289 ± 4‡‡	TD	275 ± 6	
	Nasal	267 ± 3	NV	280 ± 5 ‖	
	Temporal	284 ± 5§§	TV	310 ± 9 ‖ ‖ # # $	
Periphery	Dorsal	321 ± 8	ND	289 ± 9	326 ± 7**††
	Ventral	333 ± 14	TD	347 ± 9 ‖	
	Nasal	302 ± 10	NV	315 ± 18	
	Temporal	353 ± 9§§	TV	367 ± 20 ‖	

[1]Mean RGC soma area values in the different subregions and quadrants of regions of the porcine retina. In the right column, the mean RGC area in the whole retinal region is shown. Values are expressed as mean ± SEM of the soma area of RGCs in μm^2. ND, nasodorsal; TD, temporal-dorsal; NV, nasoventral; TV, temporal-ventral.
**$P < 0.01$ with respect to the visual streak.
††$P < 0.01$ with respect to the mid periphery.
‡‡$P < 0.01$ with respect to dorsal.
§§$P < 0.01$ with respect to nasal.
‖$P < 0.05$ and ‖ ‖$P < 0.01$ with respect to ND.
#$P < 0.01$ with respect to TD.
$$P < 0.05$ with respect to NV.

lowed by the midperiphery (274 ± 3 μm^2), with the largest values in the periphery (326 ± 7 μm^2; Table 3).

In the midperiphery, mean RGC soma area was significantly smaller in dorsal than in ventral subregions (266 ± 3 vs. 289 ± 4, $P < 0.01$). RGC area was also smaller in nasal than in temporal subregions (267 ± 3 vs. 284 ± 5, $P < 0.01$). In contrast, in the peripheral retina, mean RGC area was not significantly different between dorsal and ventral subregions (321 ± 8 vs. 333 ± 14, respectively), but it was significantly lower in the nasal than in the temporal subregion (302 ± 10 vs. 353 ± 9, $P < 0.01$; Table 3).

RGC soma size distribution

Regional differences in RGC size described above were also observed when we analyzed the distribution of soma sizes via histograms (Fig. 4). Thus, we observe a normal distribution of RGCs attending to the soma major axis length in the visual streak, with a peak at 14 μm. In this area, most RGCs (90%) have values of major axis length under 19 μm. Analysis of histograms of regions located outside the visual streak revealed that the distribution of RGCs in regions considered as midperiphery shows peaks of frequencies at different values of soma sizes. This distribution could be interpreted as a trimodal one, suggesting the presence of three RGC groups with regard to their soma size. For representative fields of the midperipheral retina, we found a first peak around 11 μm, a second peak around 15–18 μm, and a third peak of RGCs around 21 μm. Finally, for the retinal periphery, we found that most (60%) of the few RGCs present in this region have a major axis length with values above 20 μm, whereas, in the midperiphery, this percentage was 35% and, in the visual streak, than 10%.

These results demonstrate that the distribution of the different sized RGCs in the porcine retina varies with eccentricity. To analyze differences in the soma size distribution within the retina, by increasing the sample size notably, we classified RGCs into three groups on the basis of soma size and we the distribution of each through the retina. Over the whole retina, small RGCs (<15 μm) represented 11.9% ± 0.6% of all RGCs, medium-sized RGCs (15–20 μm) represented 46.1% ± 0.7% of all RGCs, and large RGCs (>20 μm) represented 42% ± 0.9% of all RGCs. Data were plotted in four gray value-coded maps, which represented the mean percentages of small, medium-sized, and large RGCs from the five retinas analyzed (Fig. 5A–C, respectively).

The percentage of small RGCs was significantly higher ($P < 0.01$) in the visual streak (28% ± 2%) than in the midperiphery (8% ± 1%) or in the periphery (3% ± 1%). The percentage of large RGCs was significantly higher ($P < 0.01$) in the periphery (65% ± 3%) compared with the midperiphery (41% ± 1%) or visual streak (23% ± 2%). Medium-sized RGCs were more homogeneously distributed throughout the retina. Only in the periphery was the percentage of medium-sized RGCs significantly lower ($P < 0.01$) than in the visual streak (32% ± 3% vs. 51% ± 1%; Fig. 6A).

When we compared the percentages of small, medium-sized, and large RGCs in the different subregions of the midperipheral retina, we found differences between the dorsal and the ventral subregions (Fig. 6B). In contrast, no significant differences were observed in the proportion of the three cell size groups between nasal and temporal hemiretinas (not shown).

On the other hand, in the peripheral retina, significant differences ($P < 0.01$) in the percentages of the different RGC types were found between nasal and temporal subregions. Thus, percentages of small and medium-sized RGCs were higher in the nasal than in the temporal retina (4% ± 1% and 40% ± 4% vs. 2% ± 1% and 25% ± 3%, respectively). In contrast, the percentage of large RGCs was lower in the nasal than in the temporal retina (57% ± 4% vs. 73% ± 3%; $P < 0.01$; Fig. 6C). No such differences were observed between the dorsal and the ventral hemiretinas.

Distribution of RGCs (Nissl staining method)

We measured the same parameters in Nissl-stained RGCs as those measured in the RGCs back-filled with Fluoro-Gold. The results obtained when analyzing the distribution of presumptive RGCs stained with toluidine blue were significantly different from those obtained when we specifically back-filled the RGCs with Fluoro-Gold. Thus, the mean RGC density estimated from Nissl-stained retinas in the midperiphery (1,192 ± 54 RGCs/mm^2) and periphery (689 ± 89 RGCs/mm^2) was significantly higher than that estimated from retinas labeled with Fluoro-Gold (699 ± 38 and 315 ± 25, respectively). In contrast, RGC density estimated in the visual streak after Nissl staining was similar to that observed with Fluoro-Gold (3,386 ± 472 vs. 3,043 ± 344 RGCs/mm^2; Table 4).

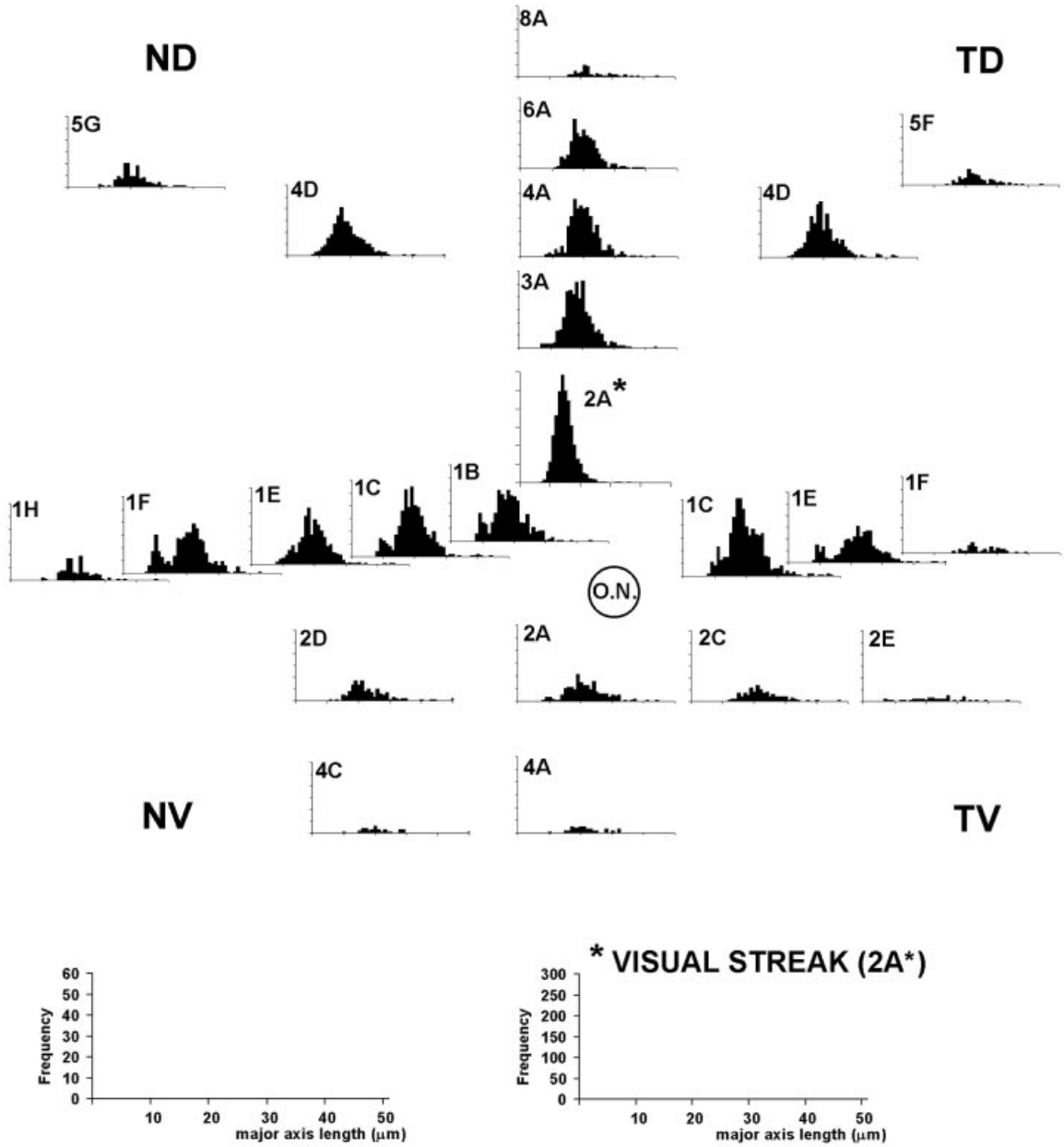

Fig. 4. Retinal ganglion cell soma size distribution as a function of eccentricity. The number of RGCs with a given major axis length was calculated in different sample fields located at different eccentricities from the optic disc (circle). The position of each sampling point is shown as a black circle in Figure 1. Bin width is 1 μm, and in total 8,008 RGCs were analyzed. Each histogram, at the different points, corresponds to the sum of frequencies for each field in the five retinas analyzed. Note that the scale used for frequencies is different for the visual streak (0–300 RGCs) and for the rest of the retina (0–60 RGCs). ND, nasodorsal; TD, temporal-dorsal; NV, nasoventral; TV, temporal-ventral; ON, optic nerve.

The distribution of the three RGC size groups is summarized in Table 5.

DISCUSSION

In the present paper, we describe the distribution of RGCs within the pig retina. The porcine retina was chosen as a suitable model, principally because of its many similarities with the human retina and because of its accessibility in comparison with nonsimian primate retinas.

For RGC density, three main regions can be distinguished in the porcine retina; the region of highest density was the visual streak, and that with the lowest density of RGCs was the periphery. This distribution has also been described for the human retina (Stone and Johnston, 1981; Curcio and Allen, 1990).

The presence of the visual streak specialization may be a general feature of mammalian topography; it has been described in nonprimates and also in primates (Stone and Johnston, 1981). Thus, although the primate retina shows

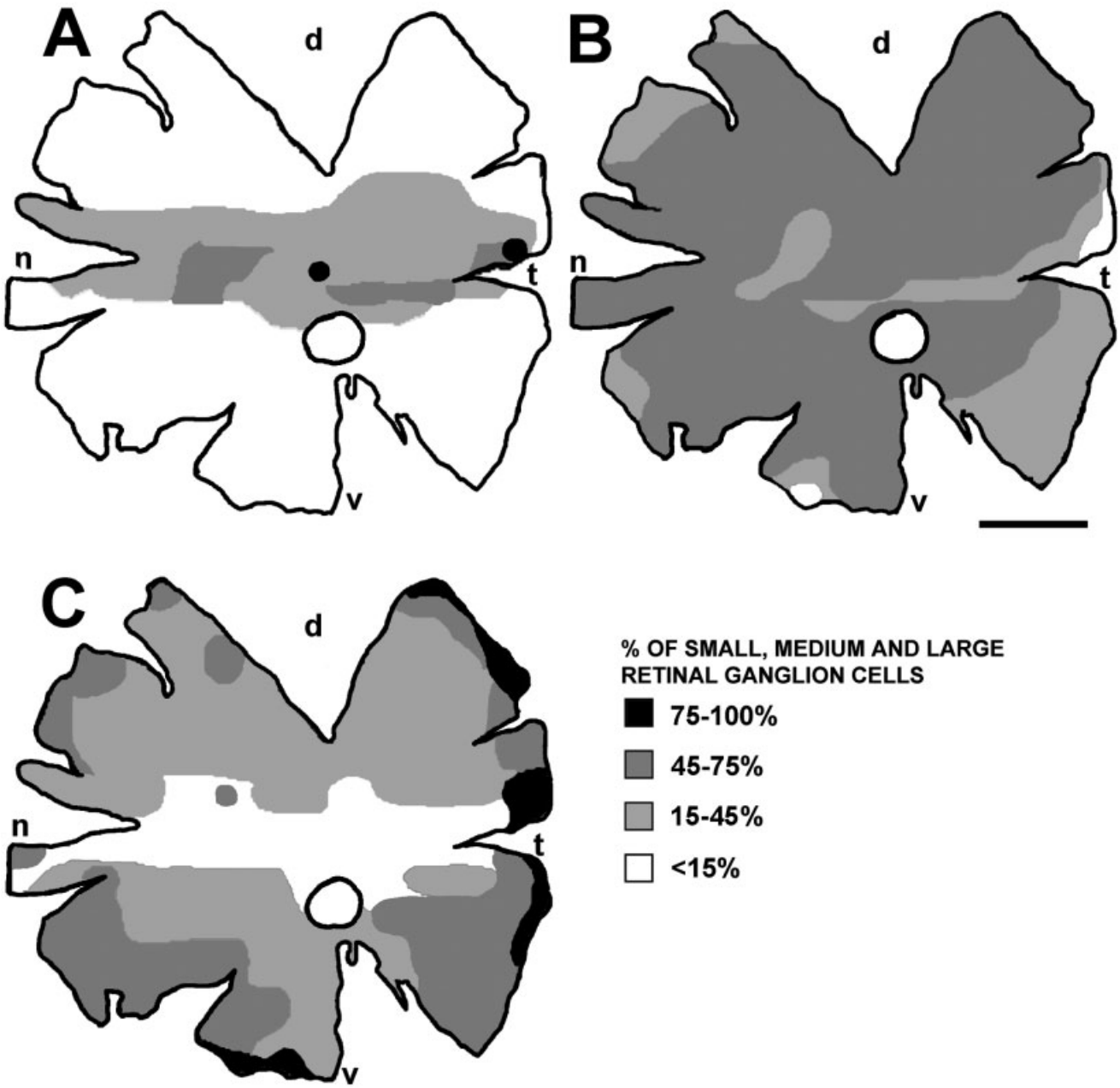

Fig. 5. Percentages of small (**A**), medium-sized (**B**), and large (**C**) retinal ganglion cells. The percentages of different-sized RGCs are represented by four gray scales, ranging from 100% (black) to less than 15% (white; see key). n, nasal; d, dorsal; t, temporal; v, ventral. Scale bar = 5 mm.

a clear foveal specialization, it has been reported that isodensity lines in ganglion cell density maps from different species of primates are horizontally elongated, suggesting the presence of a visual streak specialization. This situation is clearly apparent even in the human retina (Stone and Johnston, 1981; Curcio and Allen, 1990). Another similar feature between this proposed streak region in primates and the porcine visual streak is that, in both cases, only small branches and capillary plexuses, and not large vessels, cross the structure.

Finally, not all species of primates posses a well-developed fovea specialization; often it is relatively small (Stone and Johnston, 1981). This may be equivalent to the high density peak we observed in the porcine visual streak.

RGC density

We found that the mean density of RGCs was about 50% higher in the dorsal than in the ventral retina. Previous studies of human retina have reported that RGC density

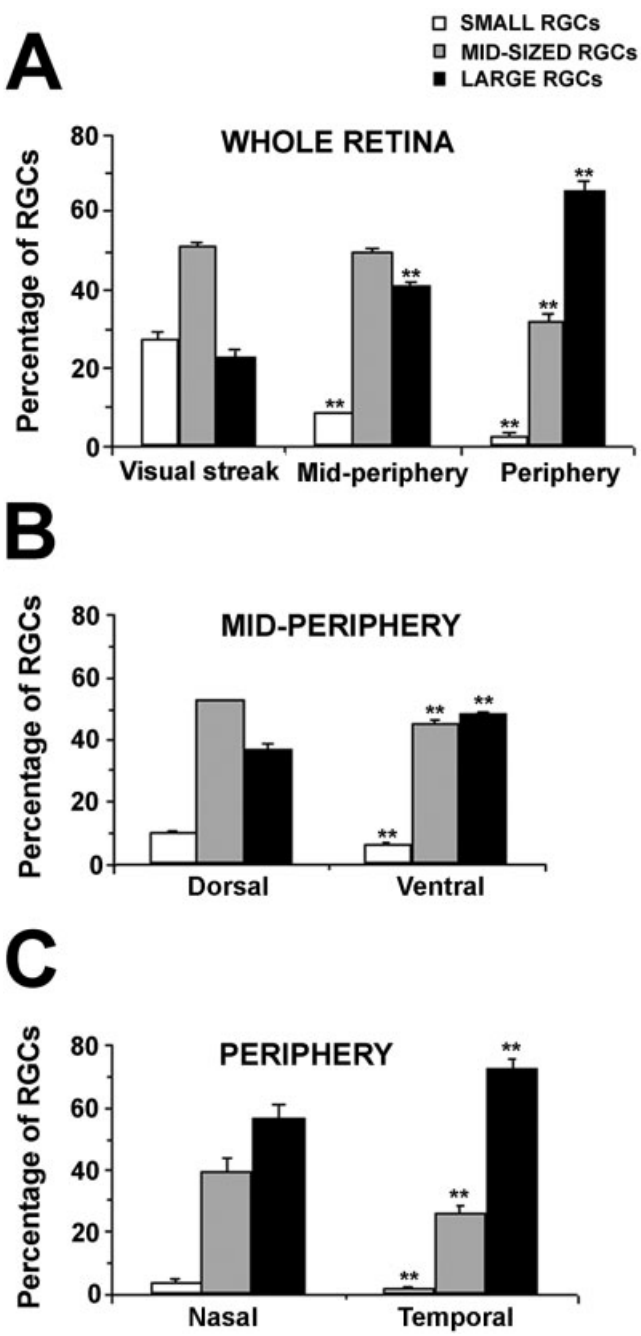

Fig. 6. Percentages of small, medium-sized, and large RGCs in different regions of the retina. **A:** RGC size distribution in the three main retinal regions: the visual streak, the midperiphery, and the periphery. $^{**}P < 0.01$, significantly different with respect to visual streak. **B:** Comparison of the RGC size distribution between the dorsal and the ventral midperipheral retina. $^{**}P < 0.01$, significantly different with respect to the dorsal retina. **C:** Comparison of the RGC size distribution between the nasal and the temporal peripheral retina. $^{**}P < 0.01$, significantly different with respect to the nasal retina. Values are expressed as the mean ± SEM of the percentages of each RGC size group.

was 60% higher in the dorsal than in the ventral retina (Curcio and Allen, 1990). With regard to nasotemporal RGC density asymmetry, similarities between human and

TABLE 4. Comparison of Mean RGC Densities (RGCs/mm^2) in the Different Retinal Regions Obtained by Fluoro-Gold and Nissl Staining Methods[1]

	Fluoro-Gold	Nissl	Nissl (Hebel, 1976)[2]
Visual streak	3,043 ± 344	3,386 ± 472	4,084
Midperiphery	699 ± 38	1,192 ± 54**	1,900
Periphery	315 ± 25	689 ± 89*	1,006

[1]Values are expressed as mean ± SEM of the number of RGCs mm^2.
[2]Data for approximated RGC density inferred from Hebel's study (1976).
$^*P < 0.05$, $^{**}P < 0.01$ with respect to Fluoro-Gold staining.

TABLE 5. Comparison of the Percentage of Small, Medium-Sized, and Large RGCs Obtained With Fluoro-Gold and Nissl Staining Methods in the Different Retinal Regions[1]

	Fluoro-Gold	Nissl
Visual streak		
Small (<14 μm)	33.06 ± 2.59	28.58 ± 3.4
Medium-sized (15–20 μm)	51.03 ± 2.02	51.36 ± 2.5
Large (>21 μm)	16.33 ± 2.07	21.43 ± 3.42
Midperiphery		
Small (<14 μm)	8.86 ± 0.71	19.34 ± 1.91**
Medium-sized (15–20 μm)	50.23 ± 1.30	41.65 ± 1.25*
Large (>21 μm)	41.11 ± 1.73	40.31 ± 2.38
Periphery		
Small (<14 μm)	3.25 ± 1.78	8.62 ± 4.05
Medium-sized (15–20 μm)	43.50 ± 9.17	30.75 ± 4.55
Large (>21 μm)	53.50 ± 9.06	60 ± 5.90

[1]Values are expressed as mean ± SEM of the percentage of RGCs.
$^*P < 0.05$, $^{**}P < 0.01$ with respect to Fluoro-Gold staining.

pig are more difficult to evaluate, because different retinal landmarks (as reference points) have been considered, and, consequently, the nomenclature used in the present work does not match that used for the human retina. Thus, previous works on human RGCs (Stone and Johnston, 1981; Curcio and Allen, 1990) use the terms *nasal* and *temporal* retina to refer to the hemiretina located nasally and temporally with respect to the foveal center, respectively, whereas we define nasal and temporal with respect to the OD (Fig. 2). Authors have described a higher mean density in nasal retina in comparison with the temporal retina (Curcio and Allen, 1990), whereas we measured a greater mean value of RGC density in the temporal than in the nasal retina. These differences probably are due to differences in the reference points used.

The fact that pig retina is endowed with a smaller number of RGCs in comparison with the human retina does not rule out the pig retina as being a good model for eye research. In fact, it has been reported that some nonhuman primate retinas, such as those of the macaque (Wässle et al., 1989), baboon (Fischer and Kirby, 1991), or cebus monkey (Silveira et al., 1989), have more RGCs than the human retina. Finally, we found that the mean area of the pig retina (781 ± 45 mm^2) is more similar to that of the human retina (883 mm^2) than that described for other primates, whose retinas have areas ranging between 319 and 527 mm^2 (Stone and Johnston, 1981).

RGC soma sizes

The trends in RGC soma size distribution among different parts of the retina described in the present work have also been reported for other species. Thus, mean RGC soma size is smaller in the central than in the peripheral retina in different species of primates. The presence of smaller cells in the central retina could be a response to the mechanical need to pack many ganglion cells into a

small region of retina, as has also been described for primates (Stone and Johnston, 1981).

Upon comparison of the nasal and temporal retina, a greater mean soma size was observed in the temporal retina than in its nasal counterpart, as has been described for the cat (Stone et al., 1980), opossum (Tancred et al., 1977; Rowe et al., 1978), fox (Rapaport et al., 1979), dog (Osmotherly, 1979), monkey, and human (Stone and Johnston, 1981) retinas. It has been suggested that these differences may reflect the different phylogenetic histories of temporal and nasal regions of the retina and that these differences may be common to all mammals.

Subtypes of RGCs have been identified in terms of several morphological or physiological criteria in mammals, and it has been described that the morphology of a specific type of RGC changes as a function of eccentricity. Thus, similar functional roles may be carried out by cells of different sizes, depending on their location within the retina (Fukuda et al., 1985; Dacey and Petersen, 1992; Yamada et al., 1996, 2001; Rockhill et al., 2002).

It is of course not possible to identify the different RGC types exclusively in terms of soma size, but by using this parameter we were able to discern a differential distribution of RGCs within different parts of the retina. Moreover, we found that, in most of the retina, frequencies of RGCs have a trimodal distribution. Previous studies on porcine retina supported the existence of three RGC soma groups with regard to the soma size (Prince et al., 1960), and we have previously found this distribution of RGCs in vitro (García et al., 2002). Indeed, the existence of three RGC size groups has previously been described in different mammalian retinas, such as the rat (Fukuda, 1977), cat (Chen and Weber, 2001), and primate (Herbin et al., 1997) retinas. Moreover, in the human retina, the presence of three frequency peaks of RGC soma diameter at 11–13, 17, and 22 μm shown by Stone and Johnston (1981) supports the existence of three distinct RGC groups. Previous studies have shown that RGCs express different cell components as a function of the size of their soma. Thus, large porcine RGCs were consistently labeled with silver staining methods attributable to the presence of large amounts of neurofilaments within their cytoskeleton (Peichl et al., 1987). However, we recently demonstrated that not only large RGCs but also small and medium-sized RGCs in the adult porcine retina express neurofilaments. Moreover, the expression of different subtypes of neurofilaments among RGCs was found to be similar, irrespective of soma size. Nevertheless, we did find differential expression of other molecules, such as neurotrophin-3, in different types of porcine RGCs (García et al., 2003).

The present morphometric analysis of RGC soma sizes in the porcine retina has revealed the existence of significant differences in soma sizes in different retinal locations, as has been reported previously for the human retina (Stone and Johnston, 1981; Curcio and Allen, 1990). In the porcine visual streak, as well as in the primate fovea, ganglion cells are more uniform in size as well as smaller than in the rest of the retina. Despite the uniformity in RGC size in these regions, it is possible that different physiological types of RGCs are present there, because studies of these cells in the macaque reported marked variation of receptive field properties and axonal conduction velocities among RGCs in the fovea (Gouras, 1969; De Monasterio, 1978).

RGC staining methods

In the present work, we used Fluoro-Gold as an efficient retrograde marker, which has been previously reported to label the entire RGC population in different species. This tracer has been successfully applied both to the superior colliculus (Berkelaar et al., 1994; Kikuchi et al., 2000; Danias et al., 2003; Hawkes et al., 2004) and to the optic nerve (Hu et al., 1999; Nakazawa et al., 2002; You et al., 2002). The Nissl staining method has been widely used to study the topography of RGCs in several species, because it is a simpler method of staining and it is not necessary to have the animal alive. However, caution should be exercised when using this technique, and it should be taken into consideration that some of the cells that are considered as RGCs may be amacrine or glial cells. In the present study, the data obtained from Nissl-stained retinas did not closely match the data obtained from Fluoro-Gold-labeled retinas. We found significant differences ($P < 0.01$) both in the density and in the size distribution of RGCs with these two methodologies. If we were to assume that most of the cells that were stained with the Nissl method but were not back-filled with Fluoro-Gold in the ganglion cell layer correspond to displaced amacrine cells, we could estimate the following: 343 displaced amacrine cells/mm^2 in the visual streak, 493 displaced amacrine cells/mm^2 in the midperiphery, and 374 displaced amacrine cells/mm^2 in the periphery. However, we cannot rule out the possibility that some of the cells stained with Nissl but not with Fluoro-Gold in the RGC layer correspond to astrocytes, which are quite abundant in this layer (Ruiz-Ederra et al., 2003).

Hebel (1976), using the Nissl staining method, obtained a higher RGC density than our estimate. These differences probably are due to tissue shrinkage, because Hebel dehydrated the retina, whereas we used PBS/glycerin-mounted retinas.

CONCLUSIONS

The distribution of porcine RGCs was found to be similar to that reported for primates in terms of cell size and distribution. Moreover, the variability in RGC distribution between individuals was found to be low. The porcine retina may be considered, on the basis of these findings, to be a useful model for ophthalmic research. The detailed characterization of the distribution of RGCs within the normal porcine retina reported in the present work will facilitate a more precise evaluation of RGC death in future studies concerning experimentally induced ocular pathologies, using the pig as a novel model.

ACKNOWLEDGMENTS

We sincerely acknowledge Francisco Martín for his skillful help with the animals.

LITERATURE CITED

Beauchemin ML. 1974. The fine structure of the pig retina. Albrecht v Graefes Arch Klin Exp Ophthalmol 190:27–45.

Berkelaar M, Clarke DB, Wang YC, Bray GM, Aguayo AJ. 1994. Axotomy results in delayed death and apoptosis of retinal ganglion cells in adult rats. J Neurosci 14:4368–4374.

Boycott BB, Wässle H. 1974. The morphological types of ganglion cells of the domestic cat's retina. J Physiol 240:397–419.

Chen H, Weber AJ. 2001. BDNF enhances retinal ganglion cell survival in cats with optic nerve damage. Invest Ophthalmol Vis Sci 42:966–974.

Curcio CA, Allen KA. 1990. Topography of ganglion cells in human retina. J Comp Neurol 300:5–25.

Dacey DM, Petersen MR. 1992. Dendritic field size and morphology of midget and parasol ganglion cells of the human retina. Proc Natl Acad Sci U S A 89:9666–9670.

Danias J, Lee KC, Zamora MF, Chen B, Shen F, Filippopoulos T, Su Y, Goldblum D, Podos SM, Mittag T. 2003. Quantitative analysis of retinal ganglion cell (RGC) loss in aging DBA/2NNia glaucomatous mice: comparison with RGC loss in aging C57/BL6 mice. Invest Ophthalmol Vis Sci 44:5151–5162.

De Monasterio FM. 1978. Properties of concentrically organized X and Y ganglion cells of macaque retina. J Neurophysiol 41:1394–1417.

De Schaepdrijver L, Lauwers H, Simoens P, De Geest JP. 1990. Development of the retina in the porcine fetus. A light microscopic study. Anat Histol Embryol 19:222–235.

Fischer QS, Kirby MA. 1991. Number and distribution of retinal ganglion cells in anubis baboons (*Papio anubis*). Brain Behav Evol 37:189–203.

Fukuda Y. 1977. A three-group classification of rat retinal ganglion cells: histological and physiological studies. Brain Res 119:327–334.

Fukuda Y, Hsiao CF, Watanabe M. 1985. Morphological correlates of Y, X and W type ganglion cells in the cat retina. Vis Res 25:319–327.

García M, Forster V, Hicks D, Vecino E. 2002. Effects of Müller glia on cell survival and neuritogenesis in adult porcine retina in vitro. Invest Ophthalmol Vis Sci 43:3735–3743.

García M, Forster V, Hicks D, Vecino E. 2003. In vivo expression of neurotrophins and neurotrophin receptors is conserved in adult porcine retina in vitro. Invest Ophthalmol Vis Sci 44:4532–4541.

Glovinsky Y, Quigley HA, Dunkelberger GR. 1991. Retinal ganglion cell loss is size dependent in experimental glaucoma. Invest Ophthalmol Vis Sci 32:484–491.

Gouras P. 1969. Antidromic responses of orthodromically identified ganglion cells in monkey retina. J Physiol 204:407–419.

Graham SL, Drance SM, Chauhan BC, Swindale NV, Hnik P, Mikelberg FS, Douglas GR. 1996. Comparison of psychophysical and electrophysiological testing in early glaucoma. Invest Ophthalmol Vis Sci 37:2651–2662.

Hawkes EL, Krueger-Naug AM, Nickerson PE, Myers TL, Currie RW, Clarke DB. 2004. Expression of Hsp27 in retinal ganglion cells of the rat during postnatal development. J Comp Neurol 478:143–148.

Hebel R. 1976. Distribution of retinal ganglion cells in five mammalian species (pig, sheep, ox, horse, dog). Anat Embryol 150:45–51.

Herbin M, Boire D, Ptito M. 1997. Size and distribution of retinal ganglion cells in the St. Kitts green monkey (*Cercopithecus aethiops sabeus*). J Comp Neurol 383:459–472.

Hu B, Yip HK, So KF. 1999. Expression of p75 neurotrophin receptor in the injured and regenerating rat retina. Neuroreport 10:1293–1297.

Joo CK, Choi JS, Ko HW, Park KY, Sohn S, Chun MH, Oh YJ, Gwag BJ. 1999. Necrosis and apoptosis after retinal ischemia: involvement of NMDA-mediated excitotoxicity and p53. Invest Ophthalmol Vis Sci 40:713–720.

Kalloniatis M, Harwerth RS, Smith EL 3rd, DeSantis L. 1993. Colour vision anomalies following experimental glaucoma in monkeys. Ophthalmic Physiol Opt 13:56–67.

Kikuchi M, Tenneti L, Lipton SA. 2000. Role of p38 mitogen-activated protein kinase in axotomy-induced apoptosis of rat retinal ganglion cells. J Neurosci 20:5037–5044.

Komáromy AM, Brooks DE, Källberg ME, Dawson WW, Szél A, Lukáts A, Samuelson DA, Sapp HL Jr, Gelatt KN, Sherwood MB. 2003. Long-term effect of retinal ganglion cell axotomy on the histomorphometry of other cells in the porcine retina. J Glaucoma 12:307–315.

Kyhn MV, Kiilgaard JF, Scherfig E, Prause J, de la Cour M. 2004. Multifocal electroretinogram (mfERG) and simultaneously monitoring of the fundus picture in the domestic pig. Invest Ophthalmol Vis Sci, vol 45, E-abstract 4247.

Li ZY, Wong F, Chang JH, Possin DE, Hao Y, Petters RM, Milam AH. 1998. Rhodopsin transgenic pigs as a model for human retinitis pigmentosa. Invest Ophthalmol Vis Sci 39:808–819.

Lieth E, Gardner TW, Barber AJ, Antonetti DA, Penn State Retina Research Group. 2000. Retinal neurodegeneration: early pathology in diabetes. Clin Exp Ophthalmol 28:3–8.

Luo X, Heidinger V, Picaud S, Lambrou G, Dreyfus H, Sahel J, Hicks D. 2001. Selective excitotoxic degeneration of adult pig retinal ganglion cells in vitro. Invest Ophthalmol Vis Sci 42:1096–1106.

Maverick KJ, Conners M, Huang A. 2004. Effect of intraocular pressure on keratometry in porcine eyes. Invest Ophthalmol Vis Sci, vol 45, E-abstract 2876.

McMenamin PG, Steptoe RJ. 1991. Normal anatomy of the aqueous humour outflow system in the domestic pig eye. J Anat 178:65–77.

Morgan JE, Uchida H, Caprioli J. 2000. Retinal ganglion cell death in experimental glaucoma. Br J Ophthalmol 84:303–310.

Nakazawa T, Tomita H, Yamaguchi K, Sato Y, Shimura M, Kuwahara S, Tamai M. 2002. Neuroprotective effect of nipradilol on axotomized rat retinal ganglion cells. Curr Eye Res 24:114–122.

Olsen TW, Sanderson S, Feng X, Hubbard WC. 2002. Porcine sclera: thickness and surface area. Invest Ophthalmol Vis Sci 43:2529–2532.

Osmotherly S. 1979. Retinal topography of the dog (*Canis familiaris*). Proc Aust Physiol Pharmacol Soc 10:143.

Peichl L, Ott H, Boycott BB. 1987. Alpha ganglion cells in mammalian retinae. Proc R Soc Lond B Biol Sci 231:169–197.

Peinado-Ramon P, Salvador M, Villegas-Perez MP, Vidal-Sanz M. 1996. Effects of axotomy and intraocular administration of NT-4, NT-3, and brain-derived neurotrophic factor on the survival of adult rat retinal ganglion cells. A quantitative in vivo study. Invest Ophthalmol Vis Sci 37:489–500.

Prince JH, Diesem CD, Eglitis I, Ruskell GL. 1960. The pig. In: Thomas CC, editor. Anatomy and histology of the eye and orbit in domestic animals. Springfield, IL: Charles C. Thomas. p 210–230.

Quigley HA, Sanchez RM, Dunkelberger GR, L'Hernault NL, Baginski TA. 1987. Chronic glaucoma selectively damages large optic nerve fibers. Invest Ophthalmol Vis Sci 28:913–920.

Quigley HA, Dunkelberger GR, Green WR. 1988. Chronic human glaucoma causing selectively greater loss of large optic nerve fibers. Ophthalmology 95:357–363.

Quigley HA, Dunkelberger GR, Green WR. 1989. Retinal ganglion cell atrophy correlated with automated perimetry in human eyes with glaucoma. Am J Ophthalmol 107:453–464.

Rapaport DH, Sesma MA, Rowe MH. 1979. Distribution and central projections of ganglion cells in the retina of the gray fox (*Urocyon cinereoargenteus*). Soc Neurosci Abstr 5:504.

Rockhill RL, Daly FJ, MacNeil MA, Brown SP, Masland RH. 2002. The diversity of ganglion cells in a mammalian retina. J Neurosci 22:3831–3843.

Rowe MH, Dreher B. 1982. Retinal W-cell projections to the medial interlaminar nucleus in the cat: implications for ganglion cell classification. J Comp Neurol 204:117–133.

Rowe MH, Rapaport DH, Wilson PD. 1978. The distribution of ganglion cells in the retina of the American opossum (*Didelphis virginiana*). Proc Aust Physiol Pharmacol Soc 9:175.

Ruiz-Ederra J, Hitchcock PF, Vecino E. 2003. Two classes of astrocytes in the adult human and pig retina in terms of their expression of high affinity NGF receptor (TrkA). Neurosci Lett 337:127–130.

Ruiz-Ederra J, García M, Hicks D, Vecino E. 2004. Comparative study of the three neurofilament subunits within pig and human retinal ganglion cells. Mol Vis 10:83–92.

Selles-Navarro I, Villegas-Perez MP, Salvador-Silva M, Ruiz-Gomez JM, Vidal-Sanz M. 1996. Retinal ganglion cell death after different transient periods of pressure-induced ischemia and survival intervals. A quantitative in vivo study. Invest Ophthalmol Vis Sci 37:2002–2014.

Silveira LC, Picanco-Diniz CW, Sampaio LF, Oswaldo-Cruz E. 1989. Retinal ganglion cell distribution in the cebus monkey: a comparison with the cortical magnification factors. Vis Res 29:1471–1483.

Stone J. 1965. A quantitative analysis of the distribution of ganglion cells in the cat's retina. J Comp Neurol 124:337–352.

Stone J. 1978. The number and distribution of ganglion cells in the cat's retina. J Comp Neurol 180:753–771.

Stone J, Clarke R. 1980. Correlation between soma size and dendritic morphology in cat retinal ganglion cells: evidence of further variation in the gamma-cell class. J Comp Neurol 192:211–217.

Stone J, Johnston E. 1981. The topography of primate retina: a study of the human, bushbaby, and New- and Old-World monkeys. J Comp Neurol 196:205–223.

Stone J, Leventhal AG, Watson CRR, Keens JS, Clarke R. 1980. Gradients between nasal and temporal retina in the properties of retina ganglion cells. J Comp Neurol 192:219–235.

Tancred E, Freeman BW, Rowe MH, Stone J. 1977. Regional specialization

in the retinas of two Australian marsupials (brush-tailed possum and scrib-wallaby). Proc Aust Physiol Pharmacol Soc 8:129.

Van Velthoven M, Willekens B, Verbraak F, de Vos K, de Smet M. 2004. Histological correlation of en-face OCT scans using a porcine retina. Invest Ophthalmol Vis Sci, vol 45, E-abstract 2371.

Vickers JC, Schumer RA, Podos SM, Wang RF, Riederer BM, Morrison JH. 1995. Differential vulnerability of neurochemically identified subpopulations of retinal neurons in a monkey model of glaucoma. Brain Res 680:23–35.

Wässle H, Illing RB. 1980. The retinal projection to the superior colliculus in the cat: a quantitative study with HRP. J Comp Neurol 190:333–356.

Wässle H, Grünert U, Röhrenbeck J, Boycott BB. 1989. Cortical magnification factor and the ganglion cell density of the primate retina. Nature 341:643–646.

Wygnanski T, Desatnik H, Quigley HA, Glovinsky Y. 1995. Comparison of ganglion cell loss and cone loss in experimental glaucoma. Am J Ophthalmol 120:184–189.

Yamada ES, Silveira LC, Perry VH. 1996. Morphology, dendritic field size, somal size, density, and coverage of M and P retinal ganglion cells of dichromatic cebus monkeys. Vis Neurosci 13:1011–1029.

Yamada ES, Silveira LC, Perry VH, Franco EC. 2001. M and P retinal ganglion cells of the owl monkey: morphology, size and photoreceptor convergence. Vis Res 41:119–131.

You SW, Bedi KS, Yip HK, So KF. 2002. Axonal regeneration of retinal ganglion cells after optic nerve pre-lesions and attachment of normal or pre-degenerated peripheral nerve grafts. Vis Neurosci 19:661–668.

Zhang L, Inoue M, Dong K, Yamamoto M. 1998. Alterations in retrograde axonal transport in optic nerve of type I and type II diabetic rats. Kobe J Med Sci 44:205–215.